ORIGINAL RESEARCH **Open access**

An AI-Driven Robotic Assembly Platform for Solid Oxide Fuel Cell Fabrication Using Imitation Learning

Reem Al-Harbi[1*], Omar Al-Qahtani[2], Salma Nasser[1]

Abstract

The energy domain, presently undergoing a digital shift spurred by computational design, is steadily transitioning towards the full automation of the pipeline from computational estimation through to device fabrication, striving to curtail reliance on protracted, hands-on trial-and-error confirmation. In the present investigation, steered by in silico density functional theory (DFT) estimations, an anthropomorphic robotic manipulator driven by artificial intelligence (AI) was ingeniously deployed to assemble clean energy apparatuses, namely solid oxide fuel cells (SOFCs). DFT projections assigned La0.35Bi0.15Sr0.5FeO3-δ (LBSF) a pronounced capability for oxygen reduction reactions (ORRs), positioning it as an apt cathode candidate for SOFCs relative to the standard La0.5Sr0.5FeO3-δ (LSF). This compound was processed into a slurry and subsequently delivered to the assembly station outfitted with AI-operated robotics. Here, an imitation learning methodology was applied, enabling the machinery to proficiently absorb competencies directly from human exemplars, thereby unburdening investigators from strenuous manual involvement. Our strategy for self-sufficient SOFC production is illustrated. To simplify prospective utilization of the station, Large Language Models (LLMs) were built in to parse commands issued by people. An RGBD camera captured optical input to recognize and localize the cathode coating zone. Thereupon, an imitation learning architecture was implemented to master the application path from manual demonstrations, with the capacity to extend to disparate scenarios. The machine-prepared single cells housing the DFT-forecasted LBSF cathode were scrutinized and yielded a power density figure of 966 mW/cm^2 at 700 °C, a value doubling that attained by LSF. Through the fusion of computational screening with an AI-directed assembly station, this work delineates a foundational stride towards the realization of an AI-steered materials laboratory, poised to drastically compress materials innovation timelines in the foreseeable future. The station furthermore stands to empower investigators with disabilities to execute their scientific visions via the behavioral cloning paradigm.

Keywords Solid oxide fuel cells (SOFCs), AI-driven assembly platform, Density functional theory (DFT), Behavior cloning approach, Large language models (LLMs)

*Correspondence:
Reem Al-Harbi
rharbi@ksu.edu.sa
[1] Department of AI-Based Energy Optimization, College of Engineering, King Saud University, Riyadh, Saudi Arabia
[2] Department of Intelligent Power Systems, College of Engineering, Qatar University, Doha, Qatar

Introduction

Monotonous benchwork routines serve as a bottleneck to swift scientific advancement. Despite the considerable efficiencies in time and expenditure offered by computational prognostication, experimentalists still grapple with repetitive procedures and contact with reagents, which fragment deep ideation. Such settings prove especially exclusionary for scholars managing disabilities and for those who are pregnant, restricting their laboratory engagement. In response, self-governing lab installations have recently been devised to take over cyclical and mundane procedures, exemplified by

This is an open access article distributed under the terms of the Creative Commons Attribution-NonCommercial-ShareAlike 4.0 International License (CC BY-NC-SA 4.0), which permits non-commercial use, distribution, reproduction, and adaptation in any medium or format, provided that appropriate credit is given to the original author(s) and source, a link to the license is provided, and any changes made are indicated. Adapted material must be distributed under the same license.

© 2022 The Author(s). | Published by Institute of Smart Energy Systems Press

platforms that orchestrate chemical synthesis. These solutions, nonetheless, tend to demand high investment and possess narrowly defined functionality. Catering to a generalized, multi-protocol lab environment, we unveiled an AI-operated manipulator arm characterized by operational simplicity and the agility to assimilate advancing, state-of-the-art experimental protocols. The convergence of first-principles computational prognostication with hands-free automated laboratories has enabled us to realize expedited experimentation that obviates direct human manipulation.

Simulation work rooted in density functional theory (DFT) is proving instrumental in high-throughput materials screening, drastically trimming the overhead of iterative empirical testing [1-5]. The descriptor known as band center theory has gained traction as an economical metric for gauging catalytic aptitude, linking intrinsic electronic traits to energetic displacement vis-à-vis the Fermi threshold [6, 7]. Within the context of cathode-side electrochemistry for oxygen-ion-conducting solid oxide fuel cells (O-SOFCs), the oxygen reduction cascade can be abstracted to the intercalation and expulsion of O2- necessary to sustain ionic transport within the perovskite lattice. At its core, this reflects the reactive proficiency of the O p-band center, expressible through the energetic gap separating the p-band centroid from the Fermi edge. This parameter has proven serviceable as an expeditious proxy for forecasting ORR efficacy and the ensuing electrical power yield [8, 9].

Mirroring the uptake of thrifty DFT-based forecasts, laboratories governed by AI and robotics are emerging as an irresistible paradigm shift poised to offload redundant manual workloads from tomorrow's scientists [10, 11]. Articulated robotic manipulators are already fixtures in contemporary facilities, most conspicuously in zones dedicated to noxious substances. Their purview has lately broadened into synthesis workflows steered by schematics derived from popular computational materials engineering pipelines [12-15]. Concurrently, large language models (LLMs) have begun penetrating scientific writing and materials forecasting tasks [16]. Notwithstanding these inroads, behaviorally cloned assistive manipulators remain absent from authentic, multi-functional experimental laboratories; likewise, LLMs are yet to become pervasive as an interface for translating spoken or written human instruction into lab actions. Consequently, cultivating AI-operated robotics within the lab sphere is paramount for crystallizing wholly self-reliant research environments and furnishing the adaptiveness needed for scaled industrial fabrication.

Herein, density functional theory (DFT) was operationalized to pinpoint superior cathode formulations anchored by p-band center rationale. AI-managed robotic manipulators were deployed for the first occasion within a solid oxide fuel cell research setting, where they executed the autonomous deposition of a newly designated cathode compound. The manipulator faithfully mimicked operator motion, precisely tracking the comparatively tiny and non-uniformly positioned electrolyte area designated for coating. It delivered complete coverage over a circular zone measuring 6 mm across while wielding a delicate applicator. Upon recapitulating manual trajectories, the manipulator mapped the coating target utilizing OpenCV [17]. A Large Language Model (LLM) was concurrently fielded to orchestrate task-specific robotic maneuvers within the protocol, tangibly liberating the investigator from manual intercession at designated junctures. Empowered by this autonomous infrastructure, the DFT-identified La0.35Bi0.15Sr0.5FeO3-δ (LBSF) material was integrated into SOFCs by the robotic manipulator, culminating in a laudable performance marked by a power density of 717.03 mW/cm2, thereby completing the iterative loop linking computational material genesis with automated physical realization.

Material Prediction and Synthesis

To devise an improved cathode composition for SOFCs, we took the established first-generation compound La0.5Sr0.5FeO3-δ (LSF) and introduced bismuth—an element widely recognized for its capacity to tune electronic configurations in diverse materials—aiming to boost oxygen reduction reactions (ORRs) [18, 19]. DFT-based calculations were performed using the Vienna ab initio simulation package VASP 6.1.1. [20]. The projected density of states (PDOS) resolved onto the O 2p orbital, as plotted in **Figure 1a**, corresponds to the most energetically stable structural arrangement shown in **Figure 1b**. Compared to the parent LSF, La0.35Bi0.15Sr0.5FeO3-δ (LBSF) manifests a valence band with a smoother contour and a broader energetic breadth, both of which are beneficial for adsorptive interactions. An additional evaluation was performed by computing the O p-band centroid of oxygen, illustrated in **Figure 1a**, to gauge

© 2022 The Author(s). | Published by Institute of Smart Energy Systems Press

the prospective ORR activity. In accordance with the theoretical framework advanced by Lee *et al*. [8], this centroid position acts as a predictive indicator for the likelihood of ORRs, since the intrinsic cathode reaction chemistry fundamentally cycles through O2- extraction and reincorporation—an abstraction that yields an exponential reduction in computational expense. The ease with which oxygen is detached and reattached serves as a measure of the material's propensity to sustain vacancy generation alongside ion transport. This concept is consistent with the widely invoked triple conduction picture for SOFC cathodes, where the ionic conductivity component—spanning both proton migration and oxygen-ion diffusion—rests upon the availability of oxygen vacancies. The descriptor also implies that a p-band centroid situated at a smaller energy separation from the Fermi edge engenders stronger bonding with adsorbates [8, 9]. With an O p-band center positioned closer to the Fermi level at −2.527 eV, LBSF is indicated to possess a superior ORR prowess relative to La0.5Sr0.5FeO3-δ (LSF). Taken together, the computational prognosis pointed toward LBSF delivering elevated ORR performance in SOFC contexts.

After these theoretical projections were completed, the target material was successfully produced [21] while retaining a perovskite architecture analogous to that of LSF. This structural fidelity was substantiated by the X-ray diffraction (XRD) trace presented in **Figure 1c**, collected on a PANalytical diffractometer in quiescent air with Cu Kα radiation, with the source operating at 40 kV and a beam current of 40 mA. Transmission electron microscopy energy-dispersive X-ray (TEM-EDX) microanalysis **(Figure 1d)** further attested that all constituent elements were uniformly dispersed throughout the particles; these observations were recorded on a STEM-2100Plus instrument from JEOL equipped with energy-dispersive X-ray spectroscopy (EDS) detectors manufactured by Thermo Fisher Scientific, USA.

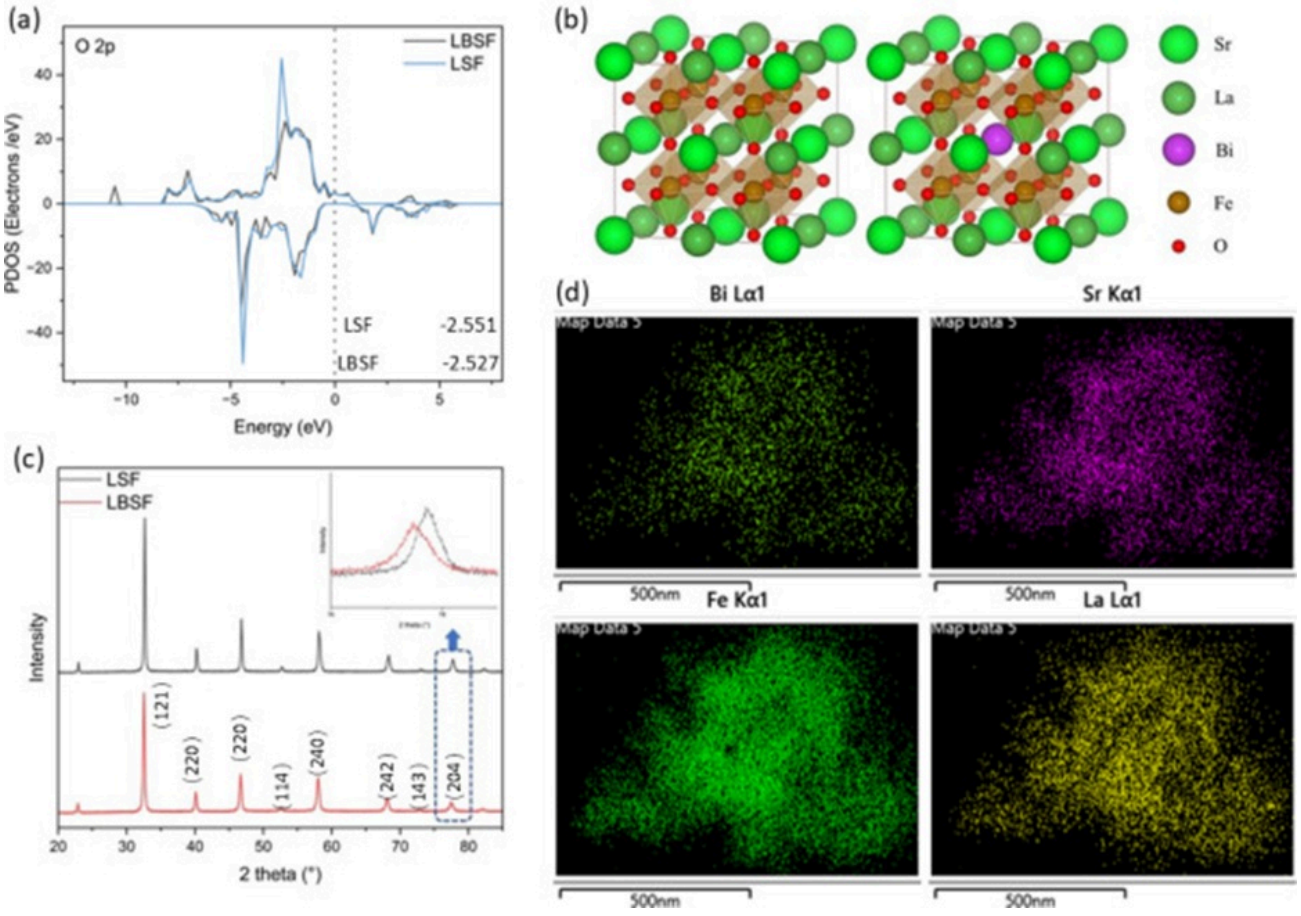

Figure 1. DFT-driven computational forecasting accompanied by successful material realization. (a) The projected density of state (PDOS) for the O 2p orbital of LSF versus LBSF. (b) Atomic-scale model representations for LSF (left) and LBSF (right). (c) XRD patterns collected for phase-pure LSF and the newly prepared LBSF. (d) Confirmation of homogeneous elemental distribution via TEM-EDX mapping.

© 2022 The Author(s). | Published by Institute of Smart Energy Systems Press

Synthesis of both La0.35Bi0.15Sr0.5FeO3-δ (LBSF) and La0.5Sr0.5FeO3-δ (LSF) proceeded via a sol–gel pathway. Stoichiometric proportions of BiN3O9 · 5 H2O (≥ 99.99%, Sigma-Aldrich), Fe(NO3)3 · 9 H2O (99.95%, Sigma-Aldrich), SrCO3 (99.9%, Sigma-Aldrich), La2O3 (99.9%, Sigma-Aldrich), citric acid monohydrate, and ethylenediaminetetraacetic acid were dissolved together in dilute nitric acid heated to 160 °C. Ammonia was then titrated into the mixture until the pH stabilized at 8. The blend was kept stirring at 160 °C for 6 h, over which period it transformed into a sol–gel, ready to be ignited into a precursor. The precursor powders of LBSF and LSF were subsequently calcined in a furnace set to 950 °C for 3 h, yielding the final product in powder form. The prepared material was subsequently converted into a cathode slurry and transferred onward to the automated assembly line for fuel cell device construction.

AI Learning for Robotic Arm Painting from Human Hands-On Teaching

AI-governed robots can learn experimental routines directly from human exemplars, enabling them to keep pace with rapidly evolving technologies and handle greater experimental throughput. In a materials research setting, any such robotic system needs a high degree of maneuverability, since tasks must be executed with tight precision inside spatially confined work envelopes. The economic aspect of the manipulator likewise looms large; a reasonably priced arm must still be able to assimilate heterogeneous motions and procedures so it can evolve alongside shifting techniques. The dual attributes of performing exacting manipulations and shifting seamlessly between dissimilar assignments are equally indispensable for AI-driven manipulators situated within lab environments.

Guided by the requirements laid out above, a manipulator destined for a fuel cell assembly station was instructed to proceed through three sequential stages, depicted schematically in **Figures 2a–2c**: The arm internalized the target operation by shadowing a human instructor during a kinesthetic teaching session, during which the teacher manually steered the limb through the set of joint configurations that define the correct motion path **(Figure 2a)**. Sensor readings logged throughout this demonstration furnished the input signals for the imitation learning pipeline. Once the control policy had been distilled from the recorded human trajectories, the manipulator replicated the expert motion at the targeted coating region. This region was autonomously identified using the Hough Circle Transform **(Figure 2b).** To accommodate a breadth of laboratory operations, LLMs were harnessed to parse the user's spoken directives **(Figure 2c)**. As soon as the utterance "painting" was registered, the arm triggered the coating sequence on its own, eliminating manual involvement throughout the procedure. After the three stages had been integrated, the platform was fully functional for deployment **(Figure 2d)**. **Figure 2b** captures a final representative usage scenario. Following the computational screening, a researcher issued a vocal command to the AI-driven robotic station, and the platform applied the new cathode slurry entirely by itself, mirroring what a human would do.

© 2022 The Author(s). | Published by Institute of Smart Energy Systems Press

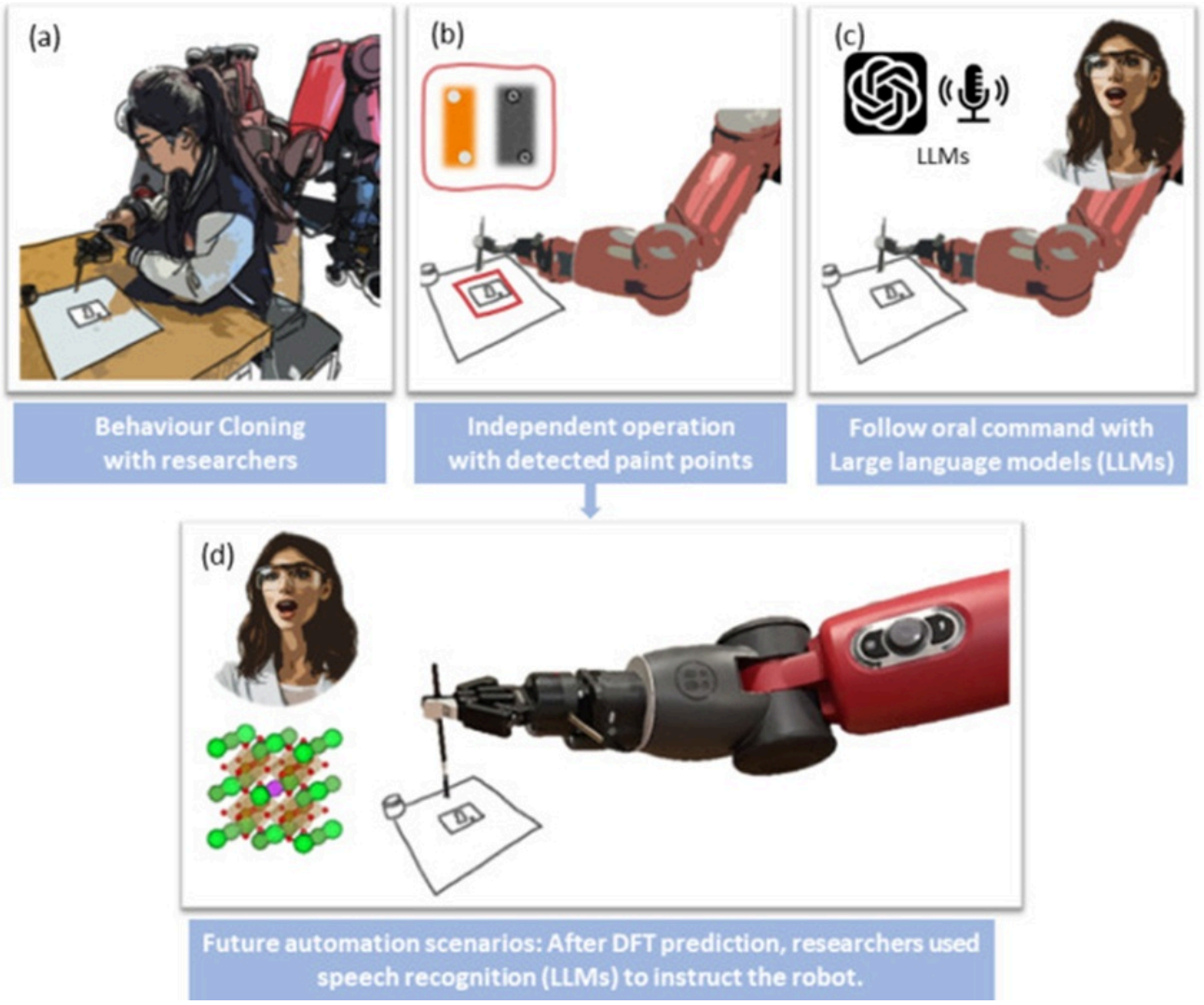

Figure 2. Three-stage pipeline for the AI robot extending from skill acquisition (a), through autonomous execution (b), to real-world application (c), along with the deployed platform in a usage setting (d).

Robot experimental setup

When implementing robotic execution, both the careful selection of the manipulator hardware and the fidelity of positional control are critical. Our choice fell upon a Baxter humanoid research robot, selected for its adaptable multifunctionality and strong capacity for adaptive learning—characteristics that render it well-suited to small-lot production. Visual sensing was delegated to an Intel RealSense D435 camera, which captures the electrode ink locations across an optimal working distance spanning 7 cm to 50 cm, delivering a spatial discrimination of up to 0.1 mm when set at 7 cm under typical interior lab illumination. An image signal processor (ISP) paired with this camera was used to augment the RGB signal, thereby making the substrate edge more distinct. This high-fidelity spatial data yields reliable positioning information, allowing the arm to zero in on the coating site without compromising the structurally delicate fuel cells.

About the fragile anode-supported half-cell pellets whose electrolyte layer measures roughly 2 m in thickness, any excessive pressing force or abrupt impact risks introducing cracks that would then choke off ionic transport. Even a hidden transverse fracture can open a path for gas crossover, which, under the operating conditions of a complete cell,

© 2022 The Author(s). | Published by Institute of Smart Energy Systems Press

could trigger a hydrogen explosion. To guard against crack initiation, every pellet was secured to a 10 × 10 cm2 Al2O3 plate, which acted as a support that spreads applied stresses. Furthermore, the brush tip employed for slurry deposition, extending about 1 cm, provides a cushioning effect that moderates the punching velocity transmitted from the robotic limb.

Robust speech recognition

Advances in natural language processing and artificial intelligence aimed at converting spoken language into text [22, 23] now permit machines to parse user commands and infer intent for personalized assistance. In the undertaking described here, we make use of Whisper [24], the open-source speech-to-text engine from OpenAI, to register painting-related commands. The robot captures an uninterrupted stream of audio, splitting it into 30 s clips and encoding these segments as .mp3 files. The default linguistic setting is English. To make Whisper effective amid background noise, the audio is first captured through a sensitive microphone, after which the Python library noisereduce is invoked to strip away ambient sound before forwarding the signal to Whisper. The model subsequently translates these files into spectrograms, tokenizes the audio passages, runs them through a transformer architecture, and decodes the result into written language. Upon identifying both “cathode” and “painting” within the transcribed segment of the current recording, the robot automatically sets the coating routine into motion, making the complete workflow entirely hands-off.

Spot identification and localization

In each painting attempt, the coordinates of the target spots are first established and spatially registered using a camera fixed to the head, together with routines from the OpenCV library [17]. As depicted in **Figure 3**, the raw frame is initially taken by the imager and then trimmed centrally down to 40% of its full extent. The trimmed picture is next rendered into a single-channel grayscale format so that noise can be suppressed and contours more readily extracted. A Hough Circle Transform is subsequently invoked to pinpoint circular features present in the image, searching within a radial span of 10 to 15 mm. A bounding rectangle is drawn snugly around each circle that is returned, and the initial waypoints along the painting track are chosen at random from inside that rectangular zone.

These starting coordinates are converted into the manipulator’s native reference frame through camera calibration and coordinate mapping procedures. Before commencing the trial, the robot positions its tool tip at the start coordinates while maintaining an upright pen grip, keeping the tool normal to the bench surface as its initial stance.

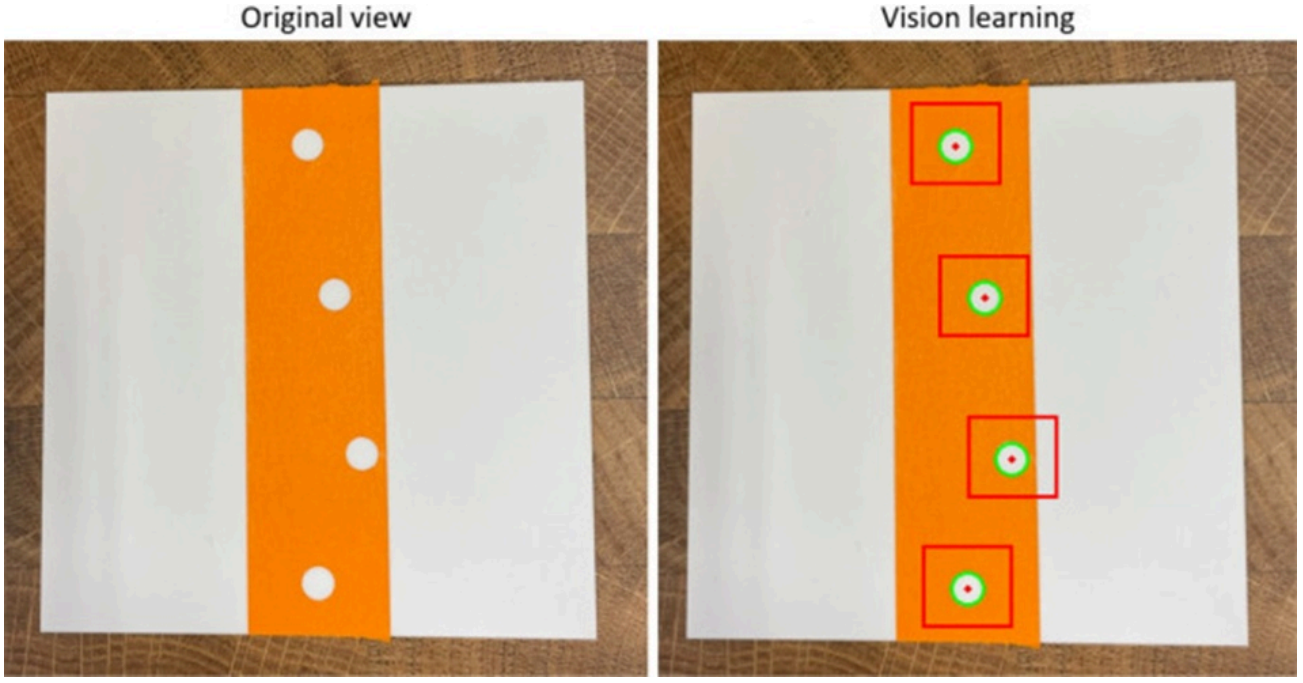

© 2022 The Author(s). | Published by Institute of Smart Energy Systems Press

Figure 3. Frame centrally trimmed to focus on the pellet (left); detected circular regions returned by the Hough Circle Transform overlaid onto the coating sites; a red bounding rectangle is placed around the identified circle (right). (For interpretation of the references to colour in this figure legend, the reader is referred to the web version of this article.)

Imitation learning of human demonstrated painting manipulation

Inside a multi-function experimental laboratory, one manipulator must handle many unrelated procedures. Taking on each of these duties requires specialist domain insight, including familiarity with complex mathematical formulations and a detailed appreciation of how the robot's dynamical response changes from one context to another. Imitation learning, built around the principle of directly copying human movement, offers robots an instinctive and uncomplicated route to absorb competencies and adjust to shifting settings **(Figure 4).**

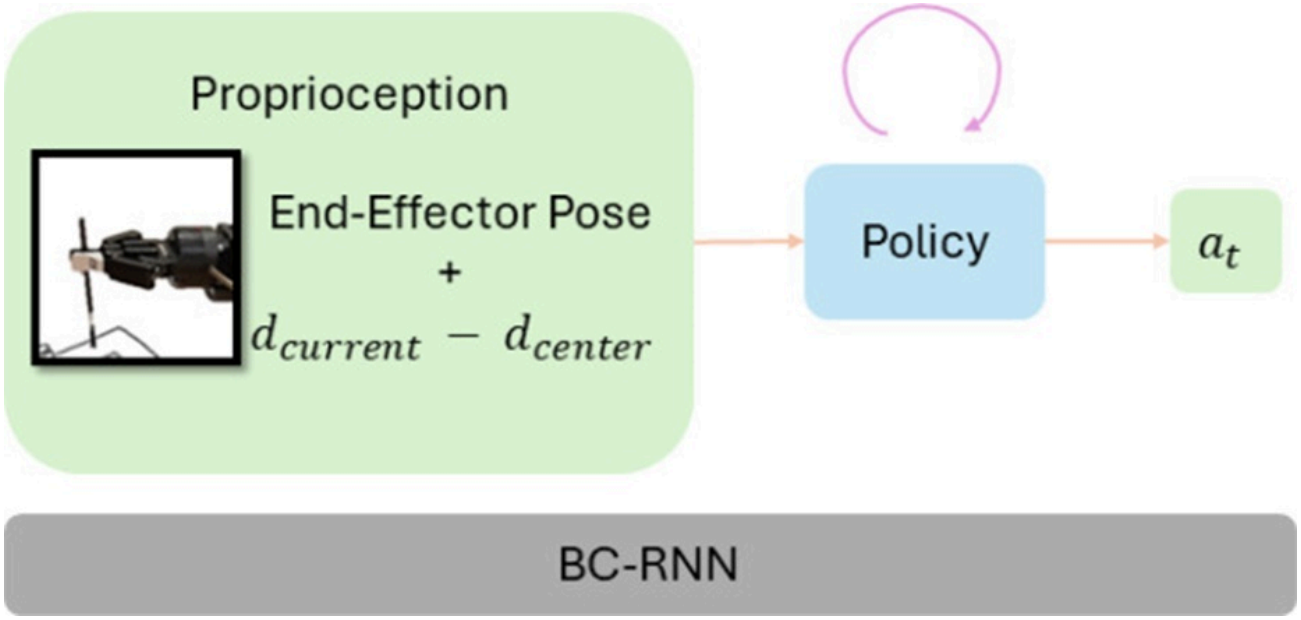

Figure 4. Schematic of our architecture: The robot captures proprioceptive readings while being kinesthetically led by a human expert; these readings comprise the instantaneous end-effector pose (3D location plus 4D quaternion) defined with respect to the original end-effector pose, together with the offset between the present end-effector location and the central painting coordinate. We apply BC-RNN to assimilate and forecast painting actions at based on the recorded demonstration motions.

© 2022 The Author(s). | Published by Institute of Smart Energy Systems Press

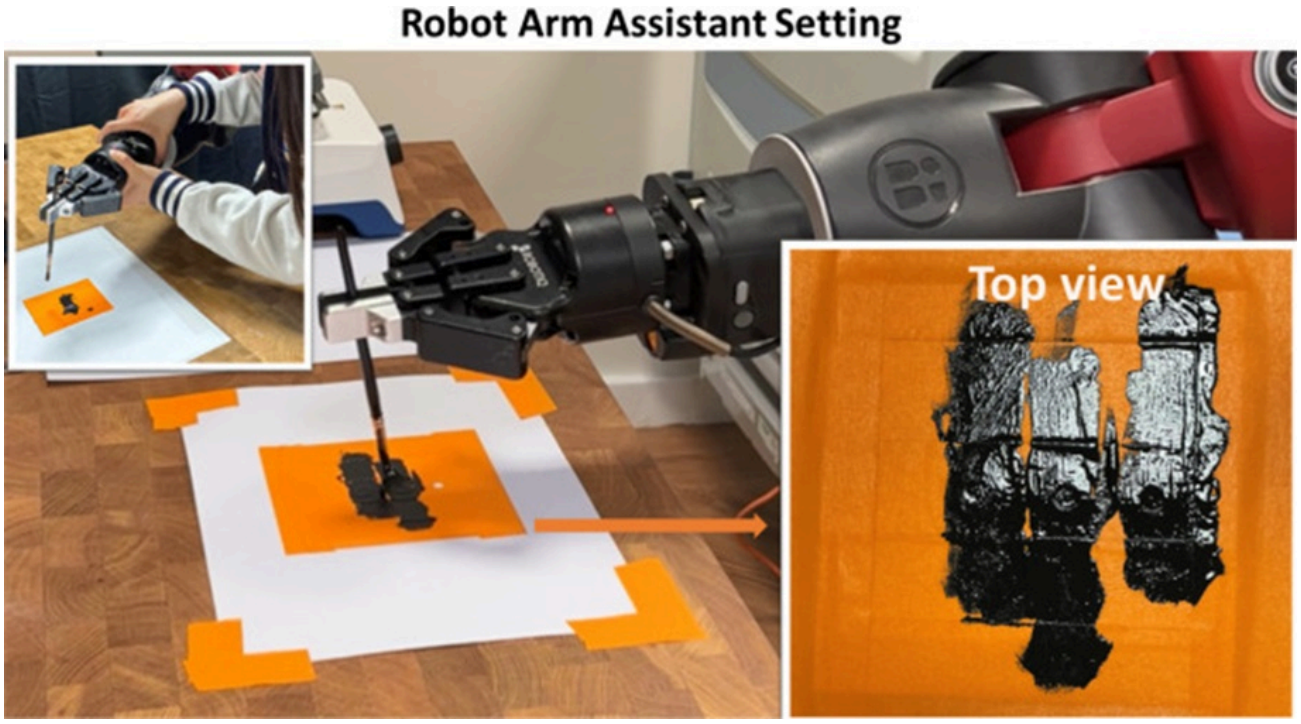

Figure 5. Human-steered robotic coaching (top left), self-sufficient robotic implementation (center), and a plan view of the deposited ink stripe (right).

Data collection

In this study, the robot is coached to reproduce human methods for applying cathode layers, as shown in **Figure 5.** We assembled 50 exemplars of coating sequences carried out on spots whose positions across the pellets were randomized. Once the manipulator settles into its starting pose, the human experts—the investigators—manually steer the arm to coat the pellet. Because these recorded sessions are meant to serve as training material for the robot to either copy or extend the displayed abilities, an Al2O3 pellet substitutes for a real cathode during the demonstration runs to save cost. The operator sweeps the arm laterally, reversing direction at each edge, until the medium uniformly blankets the intended zone and a level surface is attained. While each session was underway, the robot's internal sensory stream was logged to form the model's observation vector at every time step. This vector incorporates the ongoing end-effector configuration, expressed as a 3-dimensional position and a 4-dimensional quaternion relative to the initial end-effector pose, plus the displacement linking the current end-effector position to the centroid of the coating zone. This leaves the option to switch among null-space resolution modes when enacting elaborate painting maneuvers, and to prevent jerky, jarring limb motions that might pose a safety risk (for example, an abrupt impulsive load along the z-direction could fracture the pellets); we document the control output data. In this setup, the output is structured as a 7-dimensional vector indicating the commanded joint positions of the arm. All stored values undergo zero-centering and are rescaled so that they span the interval [−1, 1] across the entire training dataset.

Behavior cloning with a recurrent neural network approach

A parametric strategy built upon a discrete tokenization is brought to bear for translating the intricate stream of signals produced by human guidance. In this work, we implement Behavior Cloning paired with a Recurrent Neural Network (BC-RNN) as the underlying imitation learning engine. This pairing has demonstrated particular strength when learning from human-collected corpora [25, 26]. The BC-RNN module deduces actions from a time-ordered window of preceding observations through a 2-layer long short-term memory (LSTM) network. To our knowledge, this represents the first instance of imitation learning being harnessed for fully self-governing robotic arm tasks set within a materials research laboratory.

© 2022 The Author(s). | Published by Institute of Smart Energy Systems Press

The pool of recorded demonstrations was harnessed to fit a BC-RNN policy that projects observations into actions at a 30 Hz rate. The resulting actions yielded self-sufficient cathode deposition with complete coverage of the target spot when inspected from overhead **(Figure 5)**. This fitted policy was subsequently tested on real fuel cell pellets, and the appraisal results are broken down across both cathode ink microstructure and electrochemical output.

Figure 6 captures a painting product delivered by the AI robotic station after running the full sequence of three stages. We have succeeded in engineering an AI-directed technique that allows a humanoid manipulator to carry out cathode ink deposition on its own. At the beginning of each trial, the user voices a command instructing the robot to launch the routine. The linguistic content is pulled from the transcribed text via Whisper. Through parsing of contextual cues embedded in the text, the robot interprets and acts upon the user's task query. It then locates the coating target and calculates the starting pose. Steered by the policy learned through imitation, the robot carries out an uninterrupted painting trajectory absorbed from the human demonstrations. As confirmed by the head-mounted camera feed in **Figure 6**, the ink spreads to cover the circular zone entirely. Every fuel cell was then subjected to a 5-hour annealing step at 1000 °C. The deposited ink stripe emerges both flat and even, with a consistent cathode ink thickness observable in scanning electron microscope (SEM) imagery **(Figure 7)**. Distinct cathode ink formulations exhibit different degrees of surface texture. Yet, robotic deposition manages to produce an LSF surface **(Figure 7b)** every bit as smooth as that of off-the-shelf (La0.60Sr0.40)0.95Co0.20Fe0.80O3-x (LSCF) (Fuelcellmaterials: LSCF-I) **(Figure 7b).**

If this process were transferred to factory-scale output, both the brush width and the number of brushes operating in parallel could be scaled up to increase production rate without requiring additional behavior cloning training cycles, thus permitting a seamless technology handoff from laboratory to production line. The behavior cloning framework further strengthens robotic systems by allowing adaptable multilayer or triple-layer build-up, enabling parallelised multi-line manufacturing, and facilitating task expansion through incremental training in place of installing new hardware. Such a consolidated strategy substantially lowers both capital outlay and plant footprint while safeguarding processing flexibility.

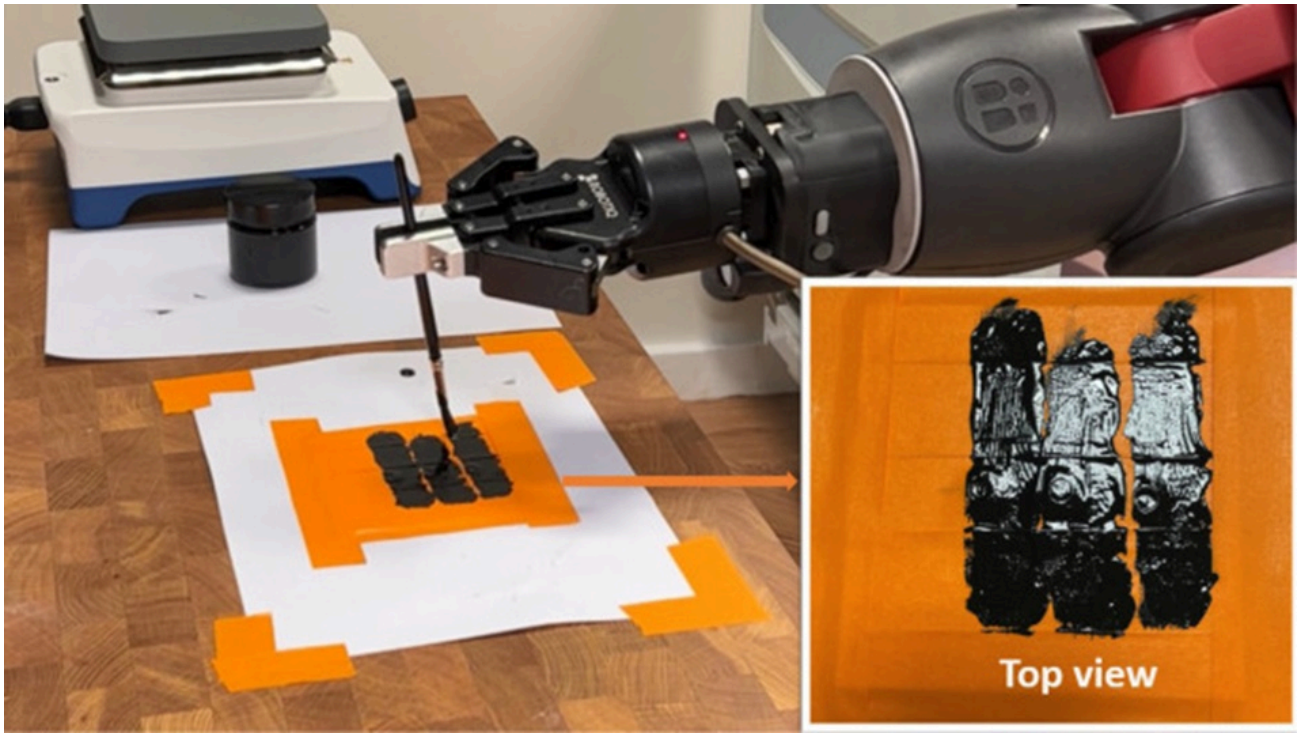

Figure 6. Hands-free robotic workflow together with an overhead view of the final ink path.

© 2022 The Author(s). | Published by Institute of Smart Energy Systems Press

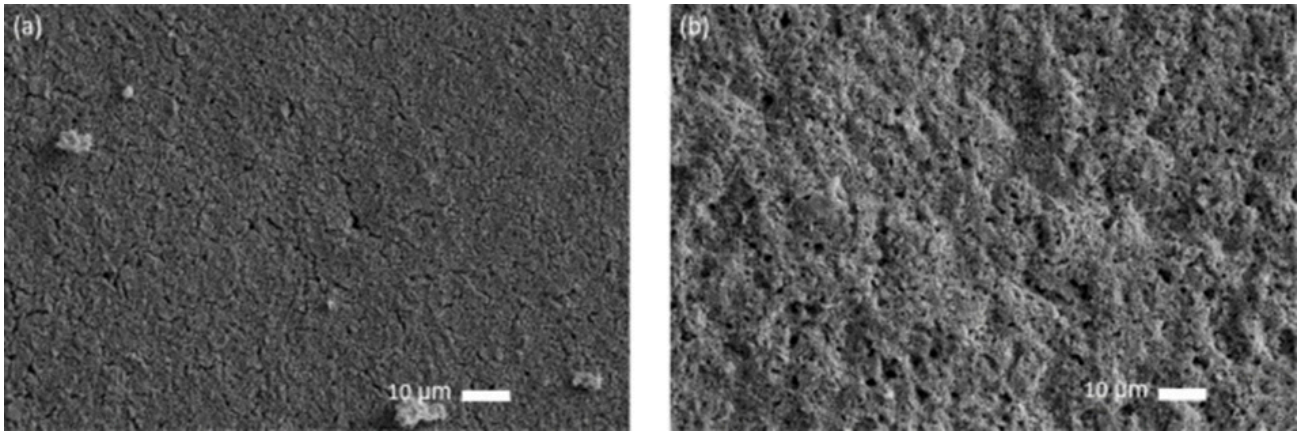

Figure 7. Overhead scanning electron microscope (SEM) views of commercial LSCF (a) and LSF (b).

Fuel Cell Tests Proved Successful Prediction Through Robotic Assistance

Guided by the DFT forecasts and the verbally issued cathode coating directive, we put the learned policy to the test for both effectiveness and transferability by tasking the robot with autonomously laying down the newly designed compound onto off-the-shelf oxygen-ion-conducting half-cells (fuelcellmaterials AEB-2.0). The resulting devices were evaluated in a fully assembled cell configuration at three temperature set points: 700, 650, and 600 °C **(Figure 8).** Operating at 700 °C, the cell built with the LBSF cathode attained a maximum power density of 966 mW / cm², a figure that comfortably outstrips the peak value of 567 mW/cm² reached by the LSF cathode under a matched set of experimental parameters. The area-specific resistance for the unoptimized single-phase LBSF registered at 0.11 Ω/cm², whereas the LSF analogue climbed markedly higher to 0.38 Ω/cm². Examination of the fracture cross-section by SEM uncovered no evidence of cracking throughout the electrolyte membrane; furthermore, the robotic deposition protocol produced excellent bonding at the interface **(Figure 8b)**. **Figure 8d** reveals a planar coating result distinguished by a layer of even thickness.

© 2022 The Author(s). | Published by Institute of Smart Energy Systems Press

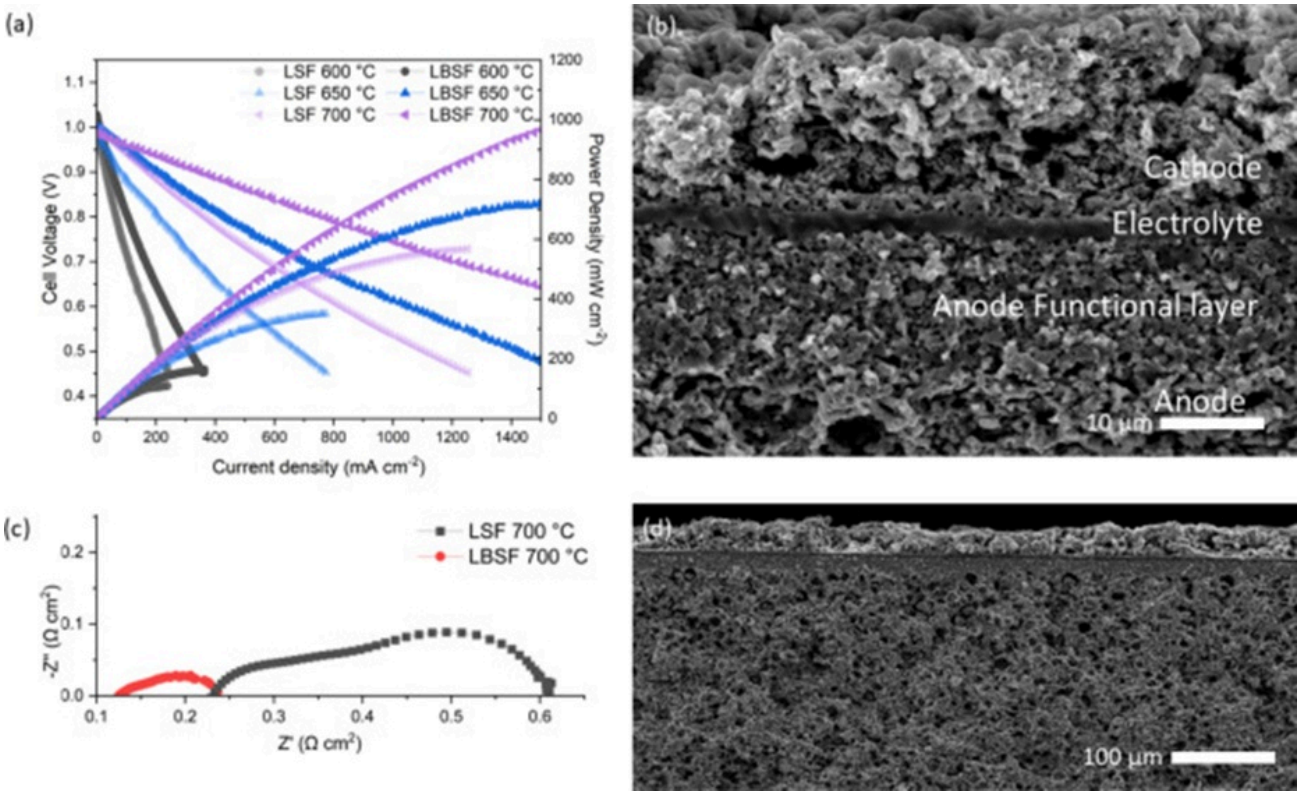

Figure 8. Fuel cell performance data showing (a) Current–voltage plots together with power density traces for single cells carrying LSF and LBSF cathodes at 700, 650, and 600 °C. (b) Cross-sectional SEM detail of the microstructure adjacent to the electrolyte region in a complete cell. (c) Impedance responses of SOFCs fitted with LSF and LBSF cathodes at 700 °C. (d) Cross-sectional SEM detail revealing a 4-layer stack configuration.

Conclusion

Conventional workflows for materials discovery are slow-moving and place a heavy burden on the scientist. In this study, a computational design route anchored in Density Functional Theory (DFT) was harnessed to prescreen cathode chemistries, drastically compressing the window ordinarily needed for candidate identification. By invoking p-band center theory as a descriptor for oxygen reduction reaction (ORR) aptitude, La0.35Bi0.15Sr0.5FeO3-δ (LBSF) was computationally projected to deliver a step-up in ORR behavior compared with LSF. The theoretically predicted compound was subsequently successfully synthesized and converted into a cathode slurry. This slurry was next entrusted to a robotic manipulation workstation which, under the direction of artificial intelligence, mirrored human technique to see the coating procedure through to completion without manual intervention, thus redeploying human effort elsewhere. Electrochemical characterization of the robot-fabricated cells was undertaken, returning a peak power density of 966 mW/cm² for the LBSF cathode. This mark handily exceeds what LSF yields under identical measurement conditions. This contribution stands as an early stride toward an AI-governed research laboratory, one in which independent robotic task execution is realized through behavioral cloning. While the ambition of a comprehensively autonomous lab remains a distant horizon, the present body of work has laid the first paving stone toward an AI-steered, closed-loop research paradigm. Forthcoming efforts will delve into expanded behavior cloning modalities that draw upon video recordings and will bring force feedback regulation into the robotic loop to uphold batch-to-batch consistency, all aimed at a self-driving laboratory in the years immediately ahead.

Acknowledgements

© 2022 The Author(s). | Published by Institute of Smart Energy Systems Press

None

Conflict of interest

None

Financial support

None

Ethics statement

None

Received: 14 Nov 2021 Revised: 22 Jan 2022 Accepted: 08 Feb 2022
Published online: 15 November 2022

Rights and permissions

Open Access The author(s) retain copyright. This article is licensed under the Creative Commons Attribution-NonCommercial-ShareAlike 4.0 International License. It may be shared and adapted for non-commercial purposes with appropriate attribution, an indication of changes, and distribution of adaptations under the same license. Third-party material may be subject to separate terms identified in its credit line. View the license at https://creativecommons.org/licenses/by-nc-sa/4.0/.

References

1. Wang Z, Wang Y, Wang J, Song Y, Robson MJ, Seong A, et al. Rational design of perovskite ferrites as high-performance proton-conducting fuel cell cathodes. Nat Catal. 2022;5(9):777-87.

2. Zhai S, Xie H, Cui P, Guan D, Wang J, Zhao S, et al. A combined ionic lewis acid descriptor and machine-learning approach to prediction of efficient oxygen reduction electrodes for ceramic fuel cells. Nat Energy. 2022;7(9):866-75.

3. Xu X, Wang H, Fronzi M, Wang X, Bi L, Traversa E. Tailoring cations in a perovskite cathode for proton-conducting solid oxide fuel cells with high performance. J Mater Chem A. 2019;7(36):20624-32.

4. Xu X, Xu Y, Ma J, Yin Y, Fronzi M, Wang X, et al. Tailoring electronic structure of perovskite cathode for proton-conducting solid oxide fuel cells with high performance. J Power Sources. 2021;489:229486.

5. Xu X, Wang H, Ma J, Liu W, Wang X, Fronzi M, et al. Impressive performance of proton-conducting solid oxide fuel cells using a first-generation cathode with tailored cations. J Mater Chem A. 2019;7(32):18792-8.

6. Hammer B, Norskov JK. Why gold is the noblest of all the metals. Nature. 1995;376(6537):238-40.

7. Nørskov JK, Abild-Pedersen F, Studt F, Bligaard T. Density functional theory in surface chemistry and catalysis. Proc Natl Acad Sci. 2011;108(3):937-43.

8. Lee YL, Kleis J, Rossmeisl J, Shao-Horn Y, Morgan D. Prediction of solid oxide fuel cell cathode activity with first-principles descriptors. Energy Environ Sci. 2011;4(10):3966-70.

9. Ji Q, Xu X, Liu X, Bi L. Improvement of the catalytic properties of porous lanthanum manganite for the oxygen reduction reaction by partial substitution of strontium for lanthanum. Electrochem Commun. 2021;124:106964.

10. Maqsood A, Chen C, Jacobsson TJ. The future of material scientists in an age of artificial intelligence. Adv Sci. 2024;2401401.

11. Adam D. The automated lab of tomorrow. Proc Natl Acad Sci. 2024;121(17):e2406320121.

12. Szymanski NJ, Rendy B, Fei Y, Kumar RE, He T, Milsted D, et al. An autonomous laboratory for the accelerated synthesis of novel materials. Nature. 2023;624(7990):86-91.

13. Chen J, Cross SR, Miara LJ, Cho JJ, Wang Y, Sun W. Navigating phase diagram complexity to guide robotic inorganic materials synthesis. Nat Synth. 2024;1-9.

14. Lunt AM, Fakhruldeen H, Pizzuto G, Longley L, White A, Rankin N, et al. Modular, multi-robot integration of laboratories: an autonomous workflow for solid-state chemistry. Chem Sci. 2024;15(7):2456-63.

15. Zhang J, Hauch JA, Brabec CJ. Toward self-driven autonomous material and device acceleration platforms (AMADAP) for emerging photovoltaics technologies. Acc Chem Res. 2024;144-52.

16. Lei G, Docherty R, Cooper SJ. Materials science in the era of large language models: a perspective. Digit Discov. 2024;3:1257-72.

17. Bradski G. The opencv library. Dr Dobb's J Softw Tools Program. 2000;25(11):120-3.

18. Niu Y, Sunarso J, Liang F, Zhou W, Zhu Z, Shao Z. A comparative study of oxygen reduction reaction on Bi- and La-doped SrFeO- perovskite cathodes. J Electrochem Soc. 2010;158(2):B132.

19. Jia W, Huang Z, Sun W, Wu L, Zheng L, Wang Y, et al. Flexible A-site doping (M=Ca, Ba, Bi; =0, 0.1, 0.2) as novel cathode material for intermediate-temperature solid oxide fuel cells: A first-principles study and experimental exploration. J Power Sources. 2021;490:229564.

20. Blaha P, Schwarz K, Madsen GK, Kvasnicka D, Luitz J. Wien2k. Augment Plane Wave+ Local Orbitals Progr Calc Cryst Prop. 2001;60(1).

21. Xu X, Bi L, Skinner SJ. Cathode surface segregating modification for boosting oxygen reduction reactions: Coupling theory and experiment in proton conducting solid oxide fuel cells (H-SOFCs). ECS Trans. 2023;111(6):1249.

22. Moor M, Banerjee O, Abad ZSH, Krumholz HM, Leskovec J, Topol EJ, et al. Foundation models for generalist medical artificial intelligence. Nature. 2023;616(7956):259-65.

23. Kaddour J, Harris J, Mozes M, Bradley H, Raileanu R, McHardy R. Challenges and applications of large language models. arXiv preprint arXiv:2307.10169. 2023.

24. Radford A, Kim JW, Xu T, Brockman G, McLeavey C, Sutskever I. Robust speech recognition via large-scale weak supervision. In: International conference on machine learning. PMLR; 2023. p. 28492-518.

25. Yu Y, Si X, Hu C, Zhang J. A review of recurrent neural networks: LSTM cells and network architectures. Neural Comput. 2019;31(7):1235-70.

26. Mandlekar A, Xu D, Wong J, Nasiriany S, Wang C, Kulkarni R, et al. What matters in learning from offline human demonstrations for robot manipulation. arXiv preprint arXiv:2108.03298. 2021.

© 2022 The Author(s). | Published by Institute of Smart Energy Systems Press